Superscaling Analyses of Inclusive Electron Scattering and Their Extension to Charge-Changing Neutrino Cross Sections in Nuclei

A. N. Antonov[1], M. V. Ivanov[1], M. K. Gaidarov[1], E. Moya de Guerra[2,3], J. A. Caballero[4], M. B. Barbaro[5], J. M. Udias[3], and P. Sarriguren[2]

[1] Institute for Nuclear Research and Nuclear Energy, Bulgarian Academy of Sciences, Sofia 1784, Bulgaria
[2] Instituto de Estructura de la Materia, CSIC, Serrano 123, 28006 Madrid, Spain
[3] Departamento de Fisica Atomica, Molecular y Nuclear, Facultad de Ciencias Fisicas, Universidad Complutense de Madrid, Madrid E-28040, Spain
[4] Departamento de Fisica Atomica, Molecular y Nuclear, Universidad de Sevilla, Apdo. 1065, 41080 Sevilla, Spain
[5] Dipartimento di Fisica Teorica, Università di Torino and INFN, Sezione di Torino, Via P. Giuria 1, 10125 Torino, Italy

Abstract. Superscaling analyses of inclusive electron scattering from nuclei are extended from the quasielastic processes to the delta-excitation region. The calculations of both quasielastic and delta longitudinal and transverse response functions as well as of $(e, e\prime)$ cross sections for ^{12}C at various incident electron energies are performed in approaches going beyond the mean-field approximation, such as the coherent density fluctuation model and that one based on the light-front dynamics method. The obtained scaling functions are used to predict charge-changing neutrino-nucleus cross sections. The analysis makes it possible to gain information about the nucleon correlation effects on both basic quantities of the nuclear ground state, the local density and the nucleon momentum distributions.

1 Introduction

The phenomenon of the scaling is observed in processes where weakly interacting probe scatters from constituents bound in a composite system and a constituent is ejected from the system in a quasifree way. A properly defined (scaling) function of a properly defined (scaling) variable turns out to depend on the nucleon momentum distribution (NMD) which is one of the basic characteristics of the nuclear ground state. The NMD is an important quantity because it is very sensitive to the nucleon-nucleon (NN) correlations in nuclei. In other words, it strongly depends on those components of the total wave function which are not accounted for in the mean-field approximation (MFA). It is known that in the MFA it is impossible to describe simultaneously the two basic nuclear characteristics, the NMD and the density distribution. Thus it is important to develop theoretical correlation methods to study these quantities beyond the MFA and to look for relevant experiments which can give information about the two quantities. We should mention that the nuclear y-scaling

analysis of inclusive electron scattering from a large variety of nuclei (*e.g.* [1–9]) showed the existence of high-momentum components in the nucleon momentum distributions $n(k)$ at momenta $k > 2$ fm^{-1} due to the presence of nucleon correlations. It was shown (see, *e.g.* [10–15]) that this specific feature of $n(k)$, which is similar for all nuclei, is a physical reason for the scaling and superscaling phenomena in nuclei. The concepts of scaling [1–9] and superscaling [10–16] have been explored in [12, 17] for extensive analyses of the (e, e') world data (see also [18]). Scaling of the first kind (no dependence on the momentum transfer) is reasonably good as expected, at excitation energies below the quasielastic (QE) peak, whereas scaling of second kind (no dependence on the mass number) is excellent in the same region. When both types of scaling behavior occur one says that the superscaling takes place. At energies above the QE peak both scaling of the first and, to a lesser extent, of the second kind are shown to be violated because of important contributions introduced by effects beyond the impulse approximation, namely, inelastic scattering [19, 20] together with correlation contributions and meson exchange currents (MEC) [21, 22]. The superscaling analyses of inclusive electron scattering from nuclei for relatively high energies (several hundred MeV to a few GeV) have recently been extended to include not only quasielastic processes, but also the region where Δ-excitation dominates [23].

It has been shown in [23] that, in contrast to the relativistic Fermi gas (RFG) model scaling function, which is symmetric, limited strictly to the region $-1 \leq \psi' \leq +1$, and with a maximum value 3/4, the empirically determined $f^{QE}(\psi')$ has a somewhat asymmetric shape with a tail that extends towards positive values of ψ' and its maximum is only about 0.6. The function $f^{\rm QE}$ calculated within the relativistic mean field [24, 25] shows a good agreement with the experimental scaling function.

The superscaling analyses and the present knowledge of inclusive electron scattering allowed one to start studies of neutrino scattering off nuclei on the same basis ([23–34]). Using the superscaling analysis of few-GeV inclusive electron-scattering data, a method was proposed in [23] to predict the inclusive νA and $\overline{\nu} A$ cross sections for the case of ^{12}C in the nuclear resonance region, thereby effectively including delta isobar degrees of freedom.

In this article we follow our method presented in [13–15] to calculate the scaling function in finite nuclei firstly within the coherent density fluctuation model (CDFM) (*e.g.*, [35]) – Section 2. As pointed out in [14], the nucleon momentum distributions $n(k)$ for various nuclei obtained in [36] within a parameter-free theoretical approach based on the light-front dynamics (LFD) method (*e.g.*, [37] and references therein) are also able to describe with a good accuracy both y- and ψ'-scaling data. So, in our present work (see also [38]) we explore both methods, CDFM and LFD, to investigate further the scaling functions (also in the Δ-region, Section 3) and their applications to analyses of electron and neutrino scattering off nuclei (Section 4).

2 Scaling Function in the Quasielastic Region

The superscaling behavior of the scaling function was firstly considered within the framework of the RFG model [10–12, 16, 17, 19] where a properly defined function of the ψ'-variable was introduced. As pointed out in [12], however, the actual nuclear dynamical content of the superscaling is more complex than that provided by the RFG model. It was observed that the experimental data have a superscaling behavior in the low-ω side (ω being the transfer energy) of the quasielastic peak for large negative values of ψ' (up to $\psi' \approx -2$), while the predictions of the RFG model are $f(\psi') = 0$ for $\psi' \leq -1$. This imposes the consideration of the superscaling in realistic finite systems. One of the approaches to do this was developed [13, 14] in the CDFM [35] which is related to the δ-function limit of the generator coordinate method [13, 39]. It was shown in [13–15] that the superscaling in nuclei can be explained quantitatively on the basis of the similar behavior of the high-momentum components of the nucleon momentum distribution in light, medium and heavy nuclei. As already mentioned, the latter is related to the effects of the NN correlations in nuclei (see, *e.g.* [35]).

In the CDFM, the total scaling function is expressed by the sum of the proton $f_p^{QE}(\psi')$ and neutron $f_n^{QE}(\psi')$ scaling functions which are determined by the proton and neutron densities $\rho_p(r)$ and $\rho_n(r)$, respectively [15]:

$$f_{p(n)}^{QE}(\psi') = \int_0^{\alpha_{p(n)}/(k_F^{p(n)}|\psi'|)} dR|F_{p(n)}(R)|^2 f_{RFG}^{p(n)}(\psi'(R)). \tag{1}$$

In Eq. (1) the proton and neutron weight functions are obtained from the corresponding proton and neutron densities (normalized to Z (or N))

$$\left|F_{p(n)}(R)\right|^2 = -\frac{4\pi R^3}{3Z(N)} \left.\frac{d\rho_{p(n)}(r)}{dr}\right|_{r=R}, \tag{2}$$

$$\alpha_{p(n)} = \left(\frac{9\pi Z(N)}{4}\right)^{1/3}, \tag{3}$$

the Fermi momentum for the protons and neutrons is calculated using the expression

$$k_F^{p(n)} = \alpha_{p(n)} \int_0^{\infty} dR \frac{1}{R} |F_{p(n)}(R)|^2 \tag{4}$$

and

$$\psi'(R) = k_F^{p(n)} \frac{R\psi'}{\alpha_{p(n)}}.$$

The RFG proton and neutron scaling functions $f_{RFG}^{p(n)}(\psi'(R))$ have the form:

$$f_{RFG}^{p(n)}(\psi'(R)) = \frac{3}{4}\left[1-\left(\frac{k_F R|\psi'|}{\alpha}\right)^2\right]\left\{1+\left(\frac{Rm_N}{\alpha}\right)^2\left(\frac{k_F R|\psi'|}{\alpha}\right)^2 \times \right.$$
$$\left. \times \left[2+\left(\frac{\alpha}{Rm_N}\right)^2 - 2\sqrt{1+\left(\frac{\alpha}{Rm_N}\right)^2}\right]\right\}, \quad (5)$$

where α and k_F are changed into $\alpha_{p(n)}$ from Eq. (3) and $k_F^{p(n)}$ from Eq. (4), respectively. The functions are normalized as follows:

$$\int_0^\infty |F_{p(n)}(R)|^2 dR = 1, \quad \int_{-\infty}^\infty f_{p(n)}^{QE}(\psi')d\psi' = 1. \quad (6)$$

Then the total scaling function can be expressed by means of both proton and neutron scaling functions:

$$f^{QE}(\psi') = \frac{1}{A}[Z f_p^{QE}(\psi') + N f_n^{QE}(\psi')] \quad (7)$$

and is normalized to unity. The same consideration can be performed equivalently on the basis of the nucleon momentum distributions for protons $n^p(k)$ and neutrons $n^n(k)$ [15].

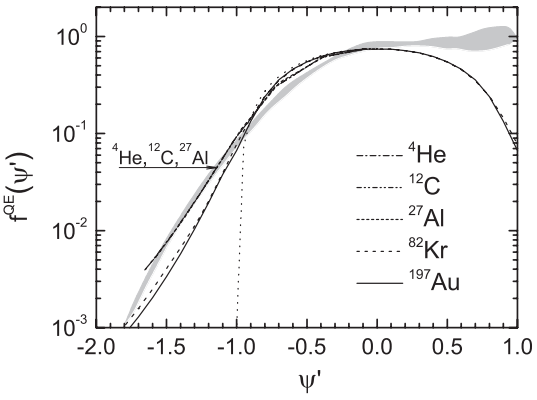

Figure **1.** The quasielastic scaling function $f^{QE}(\psi')$ at $q = 1000$ MeV/c for ^{4}He, ^{12}C, ^{27}Al, ^{82}Kr and ^{197}Au calculated in CDFM. Dotted line: RFG model result. Grey area: experimental data [11, 12].

In Figure 1 we give the QE CDFM scaling function for ^{4}He, ^{12}C, ^{27}Al, ^{82}Kr and ^{197}Au compared with experimental data and RFG results [11, 12]. As can be seen our calculations explain very well the data for $\psi' < 0$ including $\psi' < -1$ whereas in the RFG model $f(\psi') = 0$ for $\psi' \leq -1$.

In the present work we limit our approach to phenomenology when considering the asymmetric shape and the maximum value of the quasielastic scaling function. In order to simulate the role of all the effects which lead to asymmetry, we impose the latter on the RFG scaling function (and, correspondingly, on the CDFM one) by introducing a parameter which gives the correct maximum value of the scaling function (c_1 in our expressions given below) and also an asymmetry in $f^{QE}(\psi')$ for $\psi' \geq 0$. We consider the main parts of the RFG scaling function for $\psi' \leq 0$ and $\psi' \geq 0$ in the following forms, keeping the parabolic dependence on ψ' as required in [10]:

$$f^{QE}(\psi') = f_1^{QE}(\psi') + f_2^{QE}(\psi'), \tag{8}$$

where

$$f_1^{QE}(\psi') \cong \int_0^{\alpha/k_F|\psi'|} dR|F(R)|^2 c_1 \left[1 - \left(\frac{k_F R|\psi'|}{\alpha}\right)^2\right], \psi' \leq 0, \tag{9}$$

$$f_2^{QE}(\psi') \cong \int_0^{c_2\alpha/k_F|\psi'|} dR|F(R)|^2 c_1 \left[1 - \left(\frac{k_F R|\psi'|}{c_2\alpha}\right)^2\right], \psi' \geq 0. \tag{10}$$

From the normalization of $f^{QE}(\psi')$ to unity $c_2 = 3/(2c_1) - 1$.

As an example, we give in Figure 2 the CDFM QE scaling function for different values of c_1 (0.75, 0.72, 0.60 and 0.50) in comparison with the empirical data and the phenomenological fit. We also include for reference the scaling function obtained from calculations for (e, e') reaction based on the relativistic impulse approximation with FSI described using the RMF potential (see [24, 25] for details). In this way we simulate in a phenomenological way the role of the effects which violate the symmetry (and the superscaling) for positive values of ψ' of the QE scaling function including the role of the FSI.

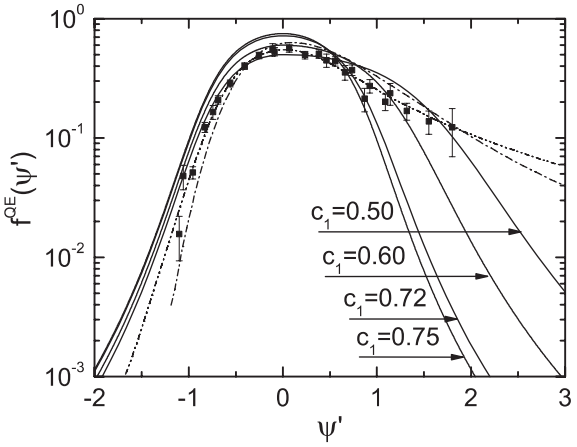

Figure **2.** The quasielastic scaling function $f^{QE}(\psi')$ for ^{12}C calculated in CDFM in comparison with the phenomenological curve which fits the data (dash-two dots), with curve fitting the result for (e, e') from [24, 25] (dash-dot line) and the experimental data (black squares) [23]. The CDFM results for different values of c_1 are also presented by solid lines.

The QE scaling function can be obtained also on the basis of the nucleon momentum distribution $n(k)$. In this work we use the modified in comparison with that from [14, 36] light-front dynamics approach presenting $n(k)$ in the form:

$$n_{\rm LFD}(k) = N_A\big[n^{\rm h}(k) + \beta\big(n_2(k) + n_5(k)\big)\big], \tag{11}$$

where $n^{\rm h}(k)$ is the hole-state (shell-model) contribution, while $n_2(k)$ and $n_5(k)$ are related to the averaged two scalar functions f_2 and f_5 [36, 37] which are part of the six components of the total deuteron function in the LFD method. The momentum distribution (11) has high-momentum components which are similar to

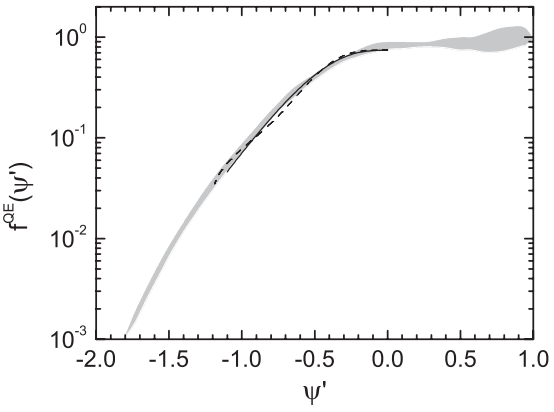

Figure **3.** The quasielastic scaling function $f^{QE}(\psi')$ calculated at $q = 1000$ MeV/c using $n_{CW}(k)$ from the y_{CW}-scaling analysis [7, 8] for ^{56}Fe (solid line) and $n_{LFD}(k)$ from modified in this work LFD approach [Eq. (11)] for ^{12}C (dashed line), with $\beta = 0.80$.

those from the y-scaling analysis [7, 8]. The calculated scaling function for ^{56}Fe at $q = 1000$ MeV/c is in agreement (see Figure 3) with the result obtained by using $n_{\rm CW}(k)$ from the $y_{\rm CW}$-scaling analysis [7, 8].

3 Scaling Function in the Quasielastic Delta Region

In this Section we extend our analysis within both CDFM and LFD to the Δ-peak region, which is not too far above the QE peak region and is the main contribution to the inelastic scattering. Following the CDFM application to the scaling phenomenon, the Δ-scaling function in the model is:

$$f^{\Delta}(\psi'_{\Delta}) = \int_0^{\infty} dR |F_{\Delta}(R)|^2 f^{\Delta}_{RFG}(\psi'_{\Delta}(R)). \tag{12}$$

In Eq. (12):

$$\psi'^{\,2}_{\Delta}(R) = \frac{1}{\left[\sqrt{1+\dfrac{k_F^2(R)}{m_N^2}}-1\right]}\left[\kappa\sqrt{\rho'^{\,2}_{\Delta}+\frac{1}{\tau'}}-\lambda'\rho'_{\Delta}-1\right] \equiv t(R).\psi'^{\,2}_{\Delta}, \tag{13}$$

where

$$t(R) \equiv \frac{\left[\sqrt{1+\dfrac{k_F^2}{m_N^2}}-1\right]}{\left[\sqrt{1+\dfrac{k_F^2(R)}{m_N^2}}-1\right]}, \quad k_F(R) = \frac{\alpha}{R}, \tag{14}$$

and $f^{\Delta}_{RFG}(\psi'_{\Delta}(R))$, ψ'_{Δ}, κ, τ', ρ'_{Δ}, λ' are defined in [23].

The results of our work are presented in Figure 4. As known, the empirical data require to use a value of the coefficient in the RFG scaling functions $f^{\Delta}_{RFG}(\psi'_{\Delta})$

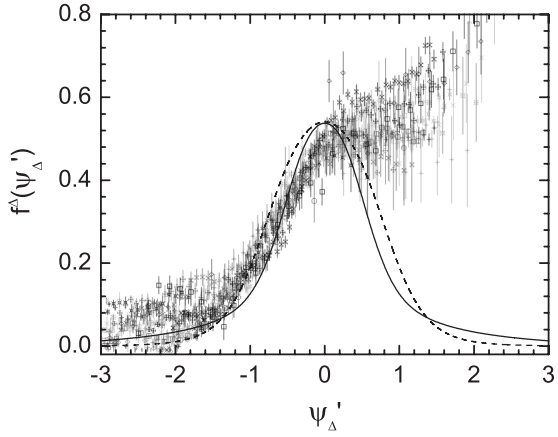

Figure **4.** The $f^{\Delta}(\psi'_{\Delta})$ scaling function for ^{12}C in the Δ-region. Dashed line: CDFM result (with $R_{\Delta} = 1.565$ fm, $b_{\Delta} = 0.420$ fm, $k_F = 1.20$ fm^{-1}); solid line: result of modified LFD approach ($\beta = 0.80$, $k_F = 1.20$ fm^{-1}). The coefficient $c_1 = 0.54$ in both CDFM and LFD cases. Averaged experimental values of $f^{\Delta}(\psi'_{\Delta})$ are taken from [23].

different from $3/4$. In our calculations in the Δ-region we use the value 0.54. We found that reasonable agreement with the data can be achieved using the parameter values given in the figure caption.

4 Scaling Functions and Inclusive Lepton Scattering

4.1 Scaling Functions and $(\mathrm{e}, \mathrm{e}')$ Reaction Cross Sections

In the one-photon-exchange approximation, the double-differential cross section in the laboratory system can be written in the form (*e.g.* [10]):

$$\frac{d^2\sigma}{d\Omega_{k'}d\epsilon'} = \sigma_M \left[\left(\frac{Q^2}{q^2} \right)^2 R_L(q,\omega) + \left(\frac{1}{2} \left| \frac{Q^2}{q^2} \right| + \tan^2 \frac{\theta}{2} \right) R_T(q,\omega) \right], \quad (15)$$

where σ_M is the Mott cross section, $Q^{\mu} = (k - k')^{\mu} = (\omega, \mathbf{q})$, $\omega = \epsilon - \epsilon'$, $q = |\mathbf{q}| = |\mathbf{k} - \mathbf{k}'|$, $Q^2 = \omega^2 - q^2 \leq 0$, k^{μ} and k'^{μ} being four-momenta of the initial and final electron. In Eq. (15) R_L and R_T are the longitudinal and transverse response functions which contain all the information on the distribution of the nuclear electromagnetic charge and current densities. These functions can be evaluated as components of the nuclear tensor $W_{\mu\nu}$. In [10] this tensor is computed in the framework of the RFG model. In the latter the nuclear response functions in both quasielastic ($X =$ QE) and Δ-resonance ($X = \Delta$) regions have the general structure

$$R_X = \frac{\mathcal{N} m_N}{q k_F} \left[R_X \right]^{\text{s.n.}} f^X_{\text{RFG}}(\psi_X), \quad (16)$$

where $\mathcal{N} = Z$ or N, $\left[R_X \right]^{\text{s.n.}}$ is the single-proton (or neutron) response function and $f^X_{\text{RFG}}(\psi_X)$ is the QE- or Δ- scaling function.

In the CDFM the longitudinal and transverse response functions can be obtained by averaging the RFG response functions in the QE- and Δ-region by means of the

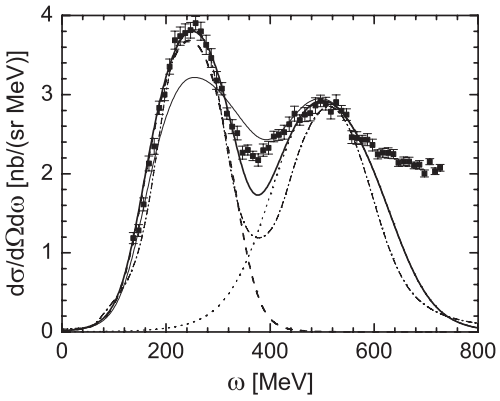

Figure **5.** Inclusive electron scattering on ^{12}C at $\epsilon = 1108$ MeV and $\theta = 37.5^\circ$ ($q^{\rm QE}_{\rm exp} \simeq 675$ MeV/c $> 2k_F$). The results obtained using $c_1^{QE} = 0.73$ in the CDFM scaling function for the QE cross section and the total result are given by dashed and thick solid line, respectively. Dotted line: using CDFM Δ-scaling function; thin solid line: total CDFM result with $c_1^{QE} = 0.63$. Dot-dashed line: using QE- and Δ-scaling functions obtained in the LFD approach. The experimental data are taken from [40].

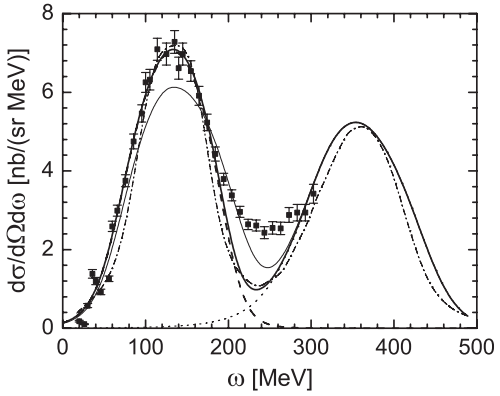

Figure **6.** Inclusive electron scattering on ^{12}C at $\epsilon = 500$ MeV and $\theta = 60^\circ$ ($q^{\rm QE}_{\rm exp} \simeq 450$ MeV/c $\gtrsim 2k_F$). The results obtained using $c_1^{QE} = 0.72$ in the CDFM scaling function for the QE cross section and the total result are given by dashed and thick solid line, respectively. Dotted line: using CDFM Δ-scaling function; thin solid line: total CDFM result with $c_1^{QE} = 0.63$. Here the dot-dashed line shows the result using QE- and Δ-scaling functions obtained in the LFD approach. The experimental data are taken from [41].

weight functions in r-space and k-space, similarly as in the case of the QE- and Δ-scaling functions. As a result, the CDFM response functions $R_{L(T)}$ in QE- and Δ-regions have approximately the same forms as in Sections 2 and 3, in which, however, the RFG scaling functions are changed by the CDFM QE- and Δ- scaling functions.

In Figures 5–7 we give examples of some results of calculations within the CDFM of inclusive electron scattering on ^{12}C at different incident energies and angles. The QE-contribution is calculated using the Fermi-type density distribution of ^{12}C with the same values of the parameters as in [13, 14]: $R = 2.47$ fm and $b = 0.42$ fm (which lead to a charge rms radius equal to the experimental one) and Fermi momentum $k_F = 1.156$ fm^{-1}. The delta-contribution is calculated using the necessary changes of the parameter values of the Fermi-type density (used in Figure 4): $R_\Delta = 1.565$ fm, $b_\Delta = 0.42$ fm and $k_F = 1.20$ fm^{-1}. The coefficient c_1 used in the Δ-region scaling function is fixed to be equal to 0.54 so that

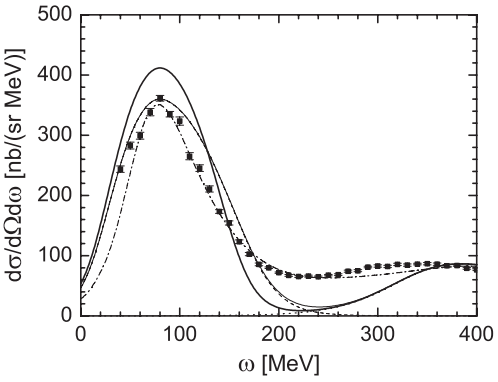

Figure **7.** Inclusive electron scattering on ^{12}C at $\epsilon = 1500$ MeV and $\theta = 13.5^\circ$ ($q_{\rm exp}^{\rm QE} \simeq 352$ MeV/c $< 2k_F$). The results obtained using $c_1^{QE} = 0.72$ in the CDFM scaling function for the QE cross section and the total result are given by dashed and thick solid line, respectively. Dotted line: using CDFM Δ-scaling function; thin solid line: total CDFM result with $c_1^{QE} = 0.63$. The dot-dashed line is the result of the ERFG approach [19, 23]. The experimental data are taken from [42].

the maximum of the scaling function to be in agreement with the data. The scaling function $f^{\Delta}(\psi'_{\Delta})$ is symmetric, its maximum is chosen to be 0.54 (but not 0.75) and it is normalized to unity by means of the fixed value of $k_F = 1.20$ fm^{-1}. The inclusive electron-^{12}C scattering cross sections shown in Figures 5–7 are the sum of the QE and Δ-contribution. The results of the CDFM calculations are presented for two values of the coefficient c_1 in the QE case (noted further by c_1^{QE}), namely for $c_1^{QE} = 0.72$ (or 0.73 in some cases) and $c_1^{QE} = 0.63$. This is related to two types of experimental data. In the first one the transferred momentum in the position of the QE peak (ω_{max}) is $q_{max}^{QE} \geq 500$ MeV/c, roughly corresponding to the domain where scaling is fulfilled. Such cases are presented in Figures 5 and 6. In these cases we found by fitting to the maximum of the QE peak the value of c_1^{QE} to be 0.72–0.73, i.e. it is not the same as in the RFG model case (case of symmetry of the RFG and of the CDFM scaling functions with $c_1^{QE} = 0.75$), but is slightly lower. This leads to a weak asymmetry of the CDFM scaling function for cases in which $q_{max}^{QE} \geq 500$ MeV/c. In the second type of experimental data q_{max}^{QE} is not in the region where condition for scaling is fulfilled ($q_{max}^{QE} < 500$ MeV/c). Such a case is given in Figure 7. For them we found by fitting to the maximum of the QE peak the value of c_1^{QE} to be 0.63. For these cases the CDFM scaling function is definitely asymmetric. So, the results in Figures 5–7 are presented for both (almost) symmetric ($c_1^{QE} = 0.72 - 0.73$) and asymmetric $c_1^{QE} = 0.63$ CDFM scaling functions. One can see that the results for the (almost) symmetric CDFM scaling function agree with the electron data in the region close to the QE peak in cases where $q_{max}^{QE} \geq 500$ MeV/c and overestimate the data for cases where approximately $q_{max}^{QE} < 500$ MeV/c. The results with asymmetric CDFM scaling function agree with the data in cases where $q_{max}^{QE} < 500$ MeV/c and underestimate the data in cases where $q_{max}^{QE} \geq 500$ MeV/c. Here we would like to emphasize that, in our opinion, the usage of asymmetric CDFM scaling function is preferable, though the results in some cases can underestimate the empirical data, because other additional effects, apart from QE and Δ-resonance (*e.g.* meson exchange currents effects) could give

important contributions to the cross section for some specific kinematics and minor for others.

In Table 1 the energies, angles, the value of c_1^{QE} obtained by fitting the magnitude of the QE peak, the energy shifts in the QE and Δ-case, as well as the approximate values of the transfer momentum q_{max}^{QE} in the position of the QE peak (ω_{max}) for different cases calculated in our work are listed. The values of the energy shifts $\epsilon_{shift}^{QE(\Delta)}$ for the QE- and Δ-regions are generally between 20 and 30 MeV. In the Figures we also present the QE-contribution (as well as Δ-contribution) for the value of c_1^{QE} which fits approximately the magnitude of the QE peak.

In Figures 5 and 6 we present also the calculations of the electron cross sections using QE- and Δ- scaling functions obtained by using the nucleon momentum distributions obtained in the LFD approach which give a reasonable agreement with the empirical electron scattering data. In Figure 7 we also give for a comparison the result of the cross sections obtained within the extended RFG (ERFG) approach [19, 23].

4.2 Scaling Functions and Charge-Changing Neutrino-Nuclei Reaction Cross Sections

In this Subsection we present applications of the CDFM and LFD scaling functions to calculations of charge-changing neutrino-nucleus reaction cross sections. We follow the description of the formalism given in [23]. The charge-changing neutrino cross section in the target laboratory frame is given in the form

$$\left[\frac{d^2\sigma}{d\Omega dk'}\right]_{\chi} \equiv \sigma_0 \mathcal{F}_{\chi}^2, \tag{17}$$

where $\chi = +$ for neutrino-induced reaction (*e.g.*, $\nu_\ell + n \to \ell^- + p$, where $\ell = e, \mu, \tau$) and $\chi = -$ for antineutrino-induced reactions (*e.g.*, $\overline{\nu}_\ell + p \to \ell^+ + n$).

Table **1.** Values of energies ϵ, angles θ, the coefficient c_1^{QE} obtained by fitting the magnitude of the QE peak, energy shifts ϵ_{shift}^{QE} and $\epsilon_{shift}^{\Delta}$, and transferred momenta $q_{\rm exp}^{\rm QE}$ for the cases of inclusive electron scattering cross sections considered. Energies are in MeV, angles are in degrees and momenta are in MeV/c.

ϵ	θ	c_1^{QE}	ϵ_{shift}^{QE}	$\epsilon_{shift}^{\Delta}$	$\approx q_{\rm exp}^{\rm QE}$
1299	37.5	0.72	30	30	792
2020	20.02	0.73	25	20	703
1108	37.5	0.73	30	30	675
620	60	0.73	20	0	552
2020	15.02	0.72	20	30	530
500	60	0.72	30	0	450
730	37.1	0.72	20	20	$442 \simeq 2k_F$
1650	13.5	0.63	20	30	390
1500	13.5	0.63	20	20	352
537	37.1	0.63	20	20	326

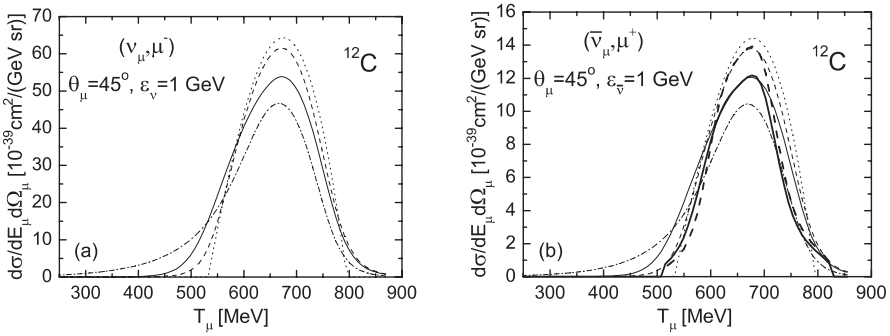

Figure **8.** The cross section of quasielastic charge-changing (ν_μ, μ^-) reaction (a) and of $(\overline{\nu}_\mu, \mu^+)$ reaction (b) on ^{12}C for $\epsilon = 1$ GeV using QE-scaling functions in CDFM (thin solid line: with $c_1 = 0.63$; thin dashed line: with $c_1 = 0.72$). The results using QE-scaling functions in LFD (thick solid line: with $c_1 = 0.63$; thick dashed line: with $c_1 = 0.72$) are presented in (b). The RFG model result and ERFG result [19, 23] are shown by dotted and dash-dotted lines, respectively.

The quantity $\mathcal{F}_\chi^2$ which depends on the nuclear structure is written in [23] as a generalized Rosenbluth decomposition having charge-charge, charge-longitudinal, longitudinal-longitudinal and two types of transverse responses. They are expanded into their vector and axial-vector contributions. The nuclear response functions are expressed in terms of the nuclear tensor $W^{\mu\nu}$ in both QE and Δ-regions using its relationships with the RFG model scaling functions. In the calculations of the neutrino-nuclei cross sections, following [23], the Höhler parametrization 8.2 [43] of the form factors in the vector sector was used, while in the axial-vector sector the form factors given in [23] were used.

In our work, instead of the RFG scaling functions in QE- and Δ-regions, we use those obtained in the CDFM and LFD approach (Sections 2 and 3). In Figure 8 we present some of the results of calculations for cross sections of QE neutrino (ν_μ, μ^-) scattering on ^{12}C and also antineutrino $(\overline{\nu}_\mu, \mu^+)$ scattering for energy of neutrino $\epsilon_\nu = 1$ GeV and of antineutrino $\epsilon_{\overline{\nu}} = 1$ GeV. The presented cross sections are functions of muon kinetic energy. The energy shift is equal to 20 MeV. We give the results of our calculations using the CDFM scaling function which is almost symmetric (with $c_1 = 0.72$), as well as the asymmetric CDFM scaling function (with $c_1 = 0.63$). These values of c_1 correspond to the cases of inclusive electron scattering considered. As can be seen the results obtained by using the almost symmetric CDFM scaling function are close to the RFG model results. On the other hand, the results obtained with the use of asymmetric CDFM and LFD scaling functions are quite different from those in the RFG model, but are close to the predictions of the ERFG model [19,23]. The basic difference from the ERFG model result is observed in the tail extended to small muon energy values, where the ERFG model gives more strength.

5 Conclusions

The results of the present work can be summarized as follows:

1. The quasielastic scaling function $f(\psi')$ is calculated in the CDFM equivalently by means of both density and nucleon momentum distributions for light, medium and heavy nuclei (including those with $Z \neq N$ for which proton and neutron densities are not similar): ^{4}He, ^{12}C, ^{27}Al, ^{56}Fe, ^{82}Kr, ^{118}Sn, ^{197}Au. The results explain the superscaling for $\psi' \leq 0$ including $\psi' < -1$, whereas in the RFG model $f(\psi') = 0$ for $\psi' \leq -1$.
2. Asymmetry in CDFM QE $f(\psi')$ is introduced phenomenologically, thus simulating the role of all the effects which violate the symmetry for $\psi' \geq 0$ including the role of FSI.
3. QE $f(\psi')$ is obtained also on the basis of nucleon momentum distributions $n(k)$ calculated within the modified light-front dynamics method. An agreement of $n_{\rm LFD}$ with the y- and $y_{\rm CW}$-scaling data is achieved, as well as a good description of the empirical QE scaling function is obtained.
4. The CDFM and LFD approaches are extended to the Δ-peak region which is the main contribution to the inelastic scattering. An agreement with the experimental data is obtained.
5. The QE- and Δ-scaling functions in CDFM and LFD are applied to description of data on inclusive electron scattering by ^{12}C at large energies and transferred momenta. The question of (almost) symmetric or asymmetric $f(\psi')$ is considered in relation to the value of $q^{\rm QE}_{\rm max}$ in the region close to the QE peak ($\omega_{\rm max}$) ($\geq$ 500 MeV/c or $<$ 500 MeV/c) and to the possibility additional effects (*e.g.* MEC) to contribute to the inclusive electron scattering cross sections for some specific kinematics.
6. The CDFM and LFD scaling functions (the same from the (e, e') analysis) are applied to calculations of charge-changing neutrino- ^{12}C (ν_μ, μ^-) and $(\overline{\nu}_\mu, \mu^+)$ reaction cross sections for energies of the incident particles from 1 to 2 GeV. The results are compared with those of RFG and ERFG methods.

Acknowledgments

Four of the authors (A.N.A., M.V.I., M.K.G., and M.B.B) are grateful to C. Giusti and A. Meucci for the discussion. This work was partly supported by the Bulgarian National Science Foundation under Contracts No.Φ-1416 and Φ-1501 and by funds provided by DGI of MCyT (Spain) under Contract Nos. FIS 2005-00640, BFM 2000-0600, BFM-04147-C02-01, FPA 2005-04460, and FIS 2005-01105.

References

1. G. B. West, *Phys. Rep.* **18**, 263 (1975).
2. I. Sick, D. B. Day, and J. S. McCarthy, *Phys. Rev. Lett.* **45**, 871 (1980).

3. D. B. Day, J. S. McCarthy, T. W. Donnelly, and I. Sick, *Annu. Rev. Nucl. Part. Sci.* **40**, 357 (1990).
4. C. Ciofi degli Atti, E. Pace, and G. Salmè, *Phys. Rev. C* **36**, 1208 (1987).
5. C. Ciofi degli Atti, E. Pace, and G. Salmè, *Phys. Rev. C* **43**, 1155 (1991).
6. C. Ciofi degli Atti and S. Simula, *Phys. Rev. C* **53**, 1689 (1996).
7. C. Ciofi degli Atti, and G. B. West, `nucl-th/9702009`.
8. C. Ciofi degli Atti and G. B. West, *Phys. Lett. B* **458**, 447 (1999).
9. D. Faralli, C. Ciofi degli Atti, and G. B. West, in *Proceedings of 2nd International Conference on Perspectives in Hadronic Physics*, ICTP, Trieste, Italy, 1999, edited by S. Boffi, C. Ciofi degli Atti and M. M. Giannini (World Scientific, Singapore, 2000), p. 75.
10. W. M. Alberico, A. Molinari, T. W. Donnelly, E. L. Kronenberg, and J. W. Van Orden, *Phys. Rev. C* **38**, 1801 (1988).
11. T. W. Donnelly and I. Sick, *Phys. Rev. Lett.* **82**, 3212 (1999).
12. T. W. Donnelly and I. Sick, *Phys. Rev. C* **60**, 065502 (1999).
13. A. N. Antonov, M. K. Gaidarov, D. N. Kadrev, M. V. Ivanov, E. Moya de Guerra, and J. M. Udias, *Phys. Rev. C* **69**, 044321 (2004).
14. A. N. Antonov, M. K. Gaidarov, M. V. Ivanov, D. N. Kadrev, E. Moya de Guerra, P. Sarriguren, and J. M. Udias, *Phys. Rev. C* **71**, 014317 (2005).
15. A. N. Antonov, M. V. Ivanov, M. K. Gaidarov, E. Moya de Guerra, P. Sarriguren, and J. M. Udias, *Phys. Rev. C* **73**, 047302 (2006).
16. M. B. Barbaro, R. Cenni, A. De Pace, T. W. Donnelly, and A. Molinari, *Nucl. Phys. A* **643**, 137 (1998).
17. C. Maieron, T. W. Donnelly, and I. Sick, *Phys. Rev. C* **65**, 025502 (2002).
18. O. Benhar, D. Day, and I. Sick, `nucl-ex/0603029`.
19. M. B. Barbaro, J. A. Caballero, T. W. Donnelly, and C. Maieron, *Phys. Rev. C* **69**, 035502 (2004).
20. L. Alvarez-Ruso, M. B. Barbaro, T. W. Donnelly, and A. Molinari, *Nucl. Phys. A* **724**, 157 (2003).
21. J. E. Amaro, M. B. Barbaro, J. A. Caballero, T. W. Donnelly, and A. Molinari, *Nucl. Phys. A* **697**, 388 (2002); **723**, 181 (2003); *Phys. Rept.* **368**, 317 (2002).
22. A. De Pace, M. Nardi, W. M. Alberico, T. W. Donnelly, and A. Molinari, *Nucl. Phys. A* **726**, 303 (2003); *ibid.* **741**, 249 (2004).
23. J. E. Amaro, M. B. Barbaro, J. A. Caballero, T. W. Donnelly, A. Molinari, and I. Sick, *Phys. Rev. C* **71**, 015501 (2005).
24. J. A. Caballero, J. E. Amaro, M. B. Barbaro, T. W. Donnelly, C. Maieron, and J. M. Udias, *Phys. Rev. Lett.* **95**, 252502 (2005).
25. J. A. Caballero, *Phys. Rev. C* **74**, 015502 (2006).
26. A. Meucci, C. Giusti, and F. D. Pacati, *Nucl. Phys. A* **744**, 307 (2004).
27. J. E. Amaro, M. B. Barbaro, J.A. Caballero, and T.W. Donnelly, *Phys. Rev. C* **73**, 035503 (2006).
28. M. C. Martinez, P. Lava, N. Jachowicz, J. Ryckebusch, and J. M. Udias, *Phys. Rev. C* **73**, 024607 (2006).
29. M. B. Barbaro, `nucl-th/0602011`.
30. J. Nieves, M. Valverde, and M. J. Vicente-Vacas, `nucl-th/0510010`.
31. M. B. Barbaro, J. E. Amaro, J. A. Caballero, T. W. Donnelly, and A. Molinari, `nucl-th/0509022`.
32. C. Maieron, M. C. Martinez, J. A. Caballero, and J. M. Udias, *Phys. Rev. C* **68**, 048501 (2003).

33. A. Meucci, C. Giusti, and F. D. Pacati, *Nucl. Phys. A* **739**, 277 (2004); **773**, 250 (2006).
34. O. Benhar, `nucl-th/0408045`; O. Benhar and N. Farina, `nucl-th/0407106`; O. Benhar, N. Farina, H. Nakamura, M. Sakuda, and R. Seki, `hep-ph/0510259`; *Phys. Rev. D* **72**, 053005 (2005).
35. A. N. Antonov, P. E. Hodgson, and I. Zh. Petkov, *Nucleon Momentum and Density Distributions in Nuclei* (Clarendon Press, Oxford, 1988); *Nucleon Correlations in Nuclei* (Springer-Verlag, Berlin-Heidelberg-New York, 1993) (and references therein).
36. A. N. Antonov, M. K. Gaidarov, M. V. Ivanov, D. N. Kadrev, G. Z. Krumova, P. E. Hodgson, and H. V. von Geramb, *Phys. Rev. C* **65**, 024306 (2002).
37. J. Carbonell and V. A. Karmanov, *Nucl. Phys. A* **581**, 625 (1995); J. Carbonell, B. Desplanques,V. A. Karmanov, and J.-F. Mathiot, *Phys. Rep.* **300**, 215 (1998).
38. A. N. Antonov, M. V. Ivanov, M. K. Gaidarov, E. Moya de Guerra, J. A. Caballero, M. B. Barbaro, J.M. Udias, and P. Sarriguren, *Phys. Rev. C* **74**, 054603 (2006); `nucl-th/0609056`.
39. J. J. Griffin and J. A. Wheeler, *Phys. Rev.* **108**, 311 (1957).
40. R. M. Sealock *et al.*, *Phys. Rev. Lett.* **62**, 1350 (1989).
41. R. R. Whitney, I. Sick, J. R. Ficenec, R. D. Kephart, and W. P. Trower, *Phys. Rev C* **9**, 2230 (1974).
42. D. T. Baran *et al.*, *Phys. Rev. Lett.* **61**, 400 (1988).
43. G. Höhler *et al.*, *Nucl. Phys. B* **114**, 505 (1976).